Effect of the second ring of antiresonant tubes in negative-curvature fibers

Wang, Yuxi; Md Imran Hasan; Muhammad Rosdi Abu Hassan; Chang, Wonkeun

2020

https://hdl.handle.net/10356/157575

https://doi.org/10.1364/OE.382516

Effect of the second ring of antiresonant tubes in negative-curvature fibers

Yuxi Wang,[1] Md Imran Hasan,[2] Muhammad Rosdi Abu Hassan,[1] and Wonkeun Chang[1,*] iD

[1]*School of Electrical and Electronic Engineering, Nanyang Technological University, Singapore 639798, Singapore*
[2]*Optical Sciences Group, Research School of Physics, The Australian National University, Acton ACT 2601, Australia*
[*]wonkeun.chang@ntu.edu.sg

Abstract: We present a numerical investigation on the effect of introducing the second ring of antiresonant tubes on the guiding properties of the negative-curvature fiber. We determine the range of structural parameters for achieving the optimum light guidance in the double-ring geometry. Our study shows that the double-ring negative-curvature fiber can improve the confinement loss by up to four orders of magnitude with considerably better bending and single-mode performance when compared to its single-ring counterpart.

1. Introduction

In hollow-core fibers, light is guided in the central hollow region [1]. This feature mitigates many constraints imposed by intrinsic properties of the waveguide materials in conventional fibers, presenting a new paradigm in fiber optics. In particular, antiresonant-guiding hollow-core fibers offer transmission across a wide spectral bandwidth with a relatively small dispersion [2]. They have attracted widespread attention in recent years, offering multitude of potential applications, e.g. in optical communications [3], high-power beam delivery [4] and gas-based light sources [5–7].

The guiding properties of the antiresonant-guiding hollow-core fiber depend largely on the cladding structure. The cladding needs to be arranged in a way that induces a large index mismatch between the core and cladding modes, as to prevent the light in the core from leaking out [8,9]. Various cladding geometries have been considered in an effort to achieve this [10,11]. Studies have found that the guidance can be substantially enhanced by having negative curvatures at the core-cladding boundary [12]. This led to the realization of low-loss hollow-core fibers that consist only of a few circular tubes around the hollow core [13]. Expanding on this idea, Yu et al. fabricated an ice-cream-cone-cladding fiber, where each negative-curvature interface is supported by two straight strands that are connected to a single point in the jacket wall [14]. Kolyadin et al. further refined the design to come up with a nodeless negative-curvature fiber [15]. It keeps a small gap between the neighboring cladding elements, and hence eliminates the loss that would otherwise appear due the resonances in the nodes [16]. Moreover, Belardi and Knight suggested the use of nested-cladding elements to supplement the antiresonant reflection, and reduce the light leakage [17]. The latest demonstrations of antiresonant-guiding hollow-core fibers with the measured transmission loss as low as a couple of dB·km^{-1} are truly remarkable achievements [18–20].

Several recent numerical reports proposed introducing another layer of antiresonant tubes in negative-curvature fibers [21–23]. We note that in broadband guiding hollow-core photonic-crystal fibers, such as kagomé fibers, having additional cladding layers cause only a minor impact on the guiding properties [24,25]. On the other hand, the effect of doing so in negative-curvature fibers has not been thoroughly studied yet. In this work, we present a comprehensive investigation

on the presence of the second ring of antiresonant tubes in negative-curvature fibers. Namely, we examine numerically the effect of changing the outer ring arrangement, such as the number and diameter of the antiresonant tubes, on the confinement loss, bending loss and single-modedness of the fiber. We also look at how the deformation in the cladding structure that may arise during the fabrication process affects the overall guidance. Our study will provide a set of guidelines for choosing the fiber design parameters that are matched for different applications.

2. Design framework

The double-ring negative-curvature fiber (DR-NCF) has two cladding rings each consisting of antiresonant tubes. An example cross-sectional structure is illustrated in Fig. 1(a). This design framework permits a number of degrees of freedom for the choice of the fiber structure. Namely, D is the diameter of the core, defined as the diameter of the biggest circle that fits in the central hollow region without overlapping the antiresonant tubes; n_1 and d_1 are the number and the diameter of antiresonant tubes in the inner ring, and n_2 and d_2 are those in the outer ring; and t is the glass-web thickness of the tubes. Note that the antiresonant tubes are evenly spaced around the core in their respective rings, and the gap between the adjacent antiresonant tubes is therefore governed entirely by the choice of D, n_1, d_1, n_2 and d_2. The thick outer jacket provides the mechanical protection, and its thickness has negligible effect on the light guidance in the core.
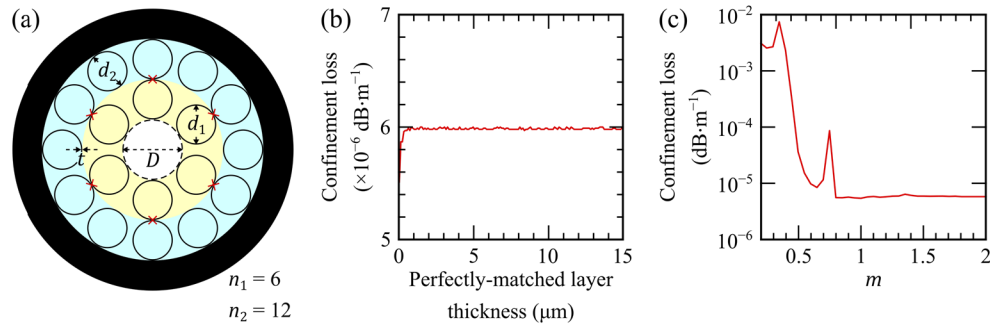

Fig. 1. (a) Idealized cross-section of a typical double-ring negative-curvature fiber (DR-NCF). D is the core diameter. t is the glass-web thickness of the antiresonant tubes. n_1 and d_1 are the number and the diameter of the antiresonant tubes in the inner ring, and n_2 and d_2 are those in the outer ring. In our numerical study, we set $D = 30\,\mu m$, $t = 0.43\,\mu m$ and $n_1 = 6$ to ensures a decent guidance at 1.06-μm wavelength, while letting d_1, n_2 and d_2 to be free parameters. Finite element modeling convergence tests for (b) the perfectly-matched layer thickness, and (c) the mesh size where the maximum mesh size in the silica and hollow regions are $\lambda_0/(6m)$ and $\lambda_0/(4m)$, respectively.

In this scheme, the annuli covered by the inner (light-yellow-shaded area) and outer (light-blue-shaded area) antiresonant tubes do not overlap as shown in Fig. 1(a). This is achieved by choosing n_2 to be an integer multiple of n_1, and ensuring every tube in the inner ring is aligned at a same azimuthal angle with one of the tubes in the outer ring. The physical support for the inner tubes is then provided by their contact points with the outer tubes, marked with red crosses in Fig. 1(a). This arrangement greatly simplifies our study, because we can change d_2 fully independent of d_1 without any overlap between the tubes. Introducing the second ring of antiresonant tubes provides additional curvatures in the cladding of the hollow-core fiber. As we shall see, this improves significantly the antiresonant reflection, ensuring a better light confinement in the core. Furthermore, it gives us an extra degree of freedom when designing the fibers that can effectively suppress or enhance the higher-order modes.

An alternative composition for the double-ring geometry is to place the inner tubes in-between two outer tubes, providing two support points for each inner tube, e.g. the two-ring split cladding fiber [26]. While such a scheme is an interesting one to analyze, its study requires an entirely different design framework defined by a different set of structural parameters. In this work, we limit the design scope of DR-NCF as outlined in Fig. 1(a).

Let us focus mainly on the light guidance at $\lambda_0 = 1.06\,\mu$m where many high-power fiber lasers are readily available. We can then further narrow down our analysis by fixing a number of design parameters; we set the core diameter at a value that is much larger than λ_0, e.g. $D = 30$ μm; the glass-web thickness can be chosen such that λ_0 is far from any resonance wavelengths, e.g. $t = 0.43\,\mu$m; and use $n_1 = 6$ for easy stacking in the fabrication process. The extent of our investigation is now clearly defined to the effect of introducing the second ring of antiresonant tubes, with only three free parameters, d_1, n_2 and d_2.

For the numerical investigation, we apply a finite-element method to calculate the confinement and bending losses for the fundamental and higher-order modes. In order to ensure our numerical accuracy and stability, we performed extensive convergence tests for various numerical parameters. Figures 1(b) and 1(c) present example convergence tests carried out for the perfectly-matched layer thickness and the maximum mesh size, respectively. The numerical simulations become stable for the layer thickness $>2\,\mu$m, and therefore we used 10-μm thick perfectly-matched layer. Moreover, the maximum mesh size for the finite-element scheme is kept below $\lambda_0/(6m)$ for the silica region and $\lambda_0/(4m)$ for the hollow region where $m = 1$, throughout this study.

3. Confinement loss

We begin our analysis by first finding d_1 that gives us the lowest confinement loss in a single-ring negative-curvature fiber (SR-NCF) with six antiresonant tubes. Shown in Fig. 2(a) is the confinement loss of its fundamental mode as a function of d_1/D. We should mention that when $d_1/D = 1$, the antiresonant tubes are in contact with each other, and therefore the ratio cannot be further increased without substantially modifying the structure.

The confinement loss decreases as d_1/D is reduced from 1, and reaches its lowest value at around $d_1/D = 0.663$. The loss increases back upon further reducing the ratio. This is because when the antiresonant tubes are too small, the gaps between the tubes become large and much of the field in the core can leak through these gaps. Nevertheless, Fig. 1(a) suggests that achieving this optimum d_1/D is not so much critical, and the loss remains relatively flat over a wide range, $0.6 < d_1/D < 0.8$. This is of practical importance and a welcoming result, for it provides a sufficient margin for the fabrication tolerance.

While setting d_1/D at its optimum value of 0.663, we now introduce the second ring of antiresonant tubes in the fiber. Figure 2(b) presents the confinement loss in the fundamental mode of DR-NCF as a function of d_2/D for $n_2 = 6$, 12, 18, 24 and 30. Notice that for each n_2, the calculation extends only up to the point marked with the vertical-dashed lines, where the outer antiresonant tubes are in contact with each other and d_2/D cannot be further increased. We can clearly see from Fig. 2(b) a remarkable reduction—by up to four orders of magnitude—in the confinement loss for DR-NCF compared to the SR-NCF. The lowest loss is obtained with $n_2 = 12$ and $d_2/D = 0.667$, where the outer ring tubes efficiently reflect the field that escaped through the gaps between the inner ring tubes back into the core. While the structure with a bigger n_2 generally results in a better confinement loss for a given d_2/D, having more tubes in the outer ring limits the maximum reachable d_2/D, which prevents the structure from achieving a lower loss. As shown in Fig. 2(a), the confinement loss as a function of d_1/D for DR-NCF when n_2 and d_2/D are fixed follows similar trend as that of SR-NCF, with the loss staying relatively low and flat across $0.6 < d_1/D < 0.8$. Therefore, the sole effect of the second ring of antiresonant tubes can reliably be investigated by keeping d_1/D within this range.
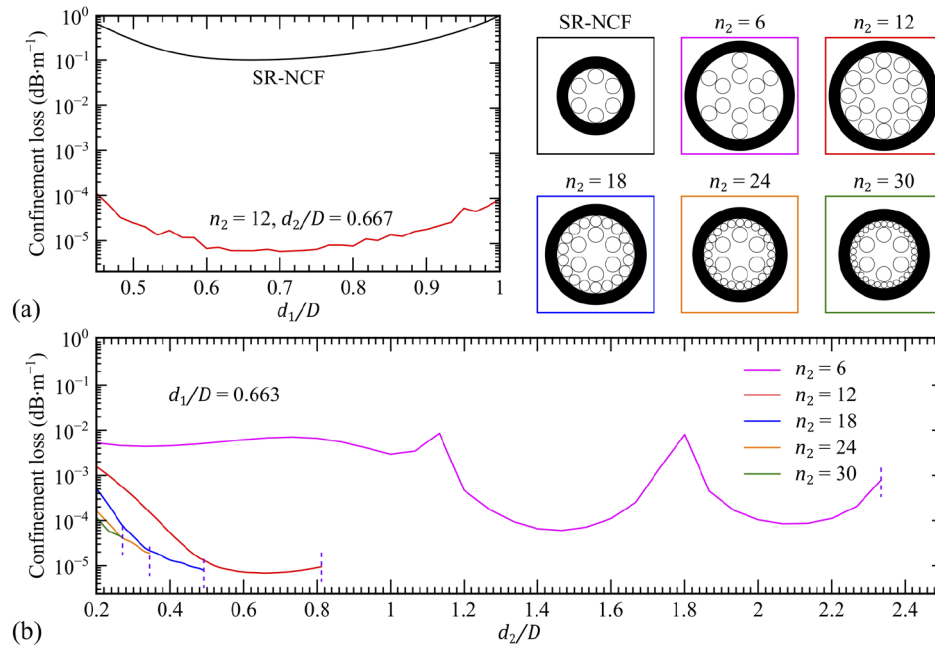
Fig. 2. (a) Confinement loss in the fundamental mode as a function of d_1/D for SR-NCF with six antiresonant tubes, and DR-NCF with $n_2 = 12$ and $d_2/D = 0.667$. (b) Confinement loss in the fundamental mode as a function of d_2/D for DR-NCF with $n_2 = 6$, 12, 18, 24 and 30. The optimum $d_1/D = 0.663$ obtained from (a) is used in the calculations. The vertical-dashed lines indicate the points where the outer ring tubes are in contact with each other. Top-right corner shows idealized cross-sections of the fibers.

We pick up from Fig. 2(b) that the performance of DR-NCF with $n_2 = 6$ is much weaker than those with higher n_2. We hence omit further analyses of the case $n_2 = 6$ in subsequent sections. For more details, we direct the readers to a recent report presenting an extensive study on this very structure for mid-infrared light guidance [27].

In Fig. 3, we reveal how DR-NCF fares against several other low-loss hollow-core fibers reported so far. The confinement loss in the spectral region between 0.9 µm and 1.6 µm is plotted for DR-NCF that resulted in the lowest loss, i.e. $d_1/D = 0.663$, $n_2 = 12$ and $d_2/D = 0.667$. This is compared with a six-tube SR-NCF, a nested antiresonant nodeless fiber (NANF) [10], a conjoined-tube fiber (CTF) [19] and a two-ring split cladding fiber (2SCF) [26]. For a fair assessment, we fix the core diameter at 30 µm and glass-web thickness in the cladding elements at 0.43 µm in all the fibers, while using the optimum values for any other structural parameters as identified in their respective literatures. Note the dramatic increase in the confinement loss of all the fibers at 0.9-µm wavelength, which is due to the resonance in the glass-web at the core-cladding boundary.

At 1.06-µm wavelength, DR-NCF clearly outperforms the other fibers. In fact, it is possible to achieve around two orders of magnitude reduction in the loss (in dB per unit length) when compared to NANF and CTF. The improvement is rather small against 2SCF, which shares many structural similarities with DR-NCF. At longer wavelengths, the confinement loss of DR-NCF increases rapidly resulting in narrower transmission bandwidth. This is due to the presence of the contact points between the tubes in the inner and outer rings that act as additional resonators. A similar transmission feature is also observable in 2SCF, which has the contact points very much alike. Nevertheless, despite the reduction in the width of the transmission window, the ultra-low
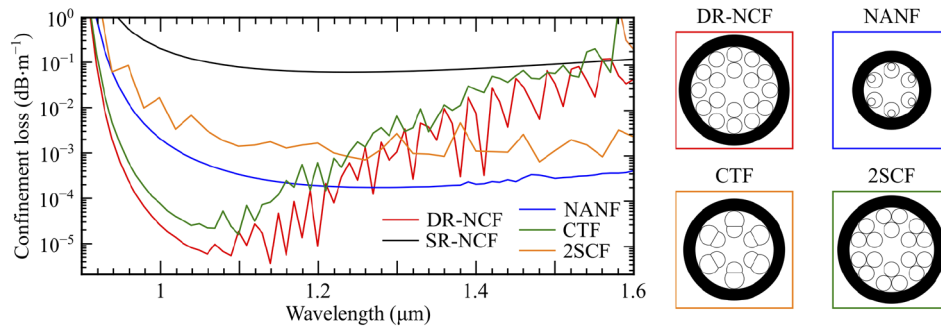
Fig. 3. Comparison of the confinement loss between SR-NCF, a nested-element nodeless fiber (NANF), a conjoined-tube fiber (CTF), a two-ring split cladding fiber (2SCF) and DR-NCF with $n_2 = 12$, $d_1/D = 0.663$ and $d_2/D = 0.667$. The right-hand side panel illustrates idealized cross-sections of these fibers.

loss offered by DR-NCF can lead to many interesting applications, particularly for high-power optical beam delivery.

4. Bending loss

Bending loss is another key fiber characteristic. It is a measure of how well the light is guided around corners—one of the main advantages of fiber optics. The bending loss performance of DR-NCF is studied, and the results are presented in Fig. 4. We use the equivalent index model for the bending loss calculations, which is given by $n' = n(1 + x/R_c)$ [28]. Here, n' is the equivalent refractive index under the bending at point x where x is the position along the bending direction from the fiber center. n is the index of the material under no stress and R_c is the radius of curvature. Note that we apply bending in the horizontal direction for all bending loss calculations. The bend-induced loss as presented in the vertical axes in Fig. 4 is obtained by subtracting the confinement loss in the fundamental mode of the straight fiber from that of the bent fiber. By doing so, we can isolate only the sole contribution of the bend on the loss. We first set $R_c = 7$ cm to understand the effect of changing the structural parameters on the bend-induced loss. We find this choice of the bending radius adequate for effectively exposing the impact of bending for the range of structural parameters used in our study. Moreover, we consider $R_c = 7$ cm an acceptable value for most tabletop-scale experiments.

Figure 4(a) plots the bend-induced loss as a function of d_2/D for $n_2 = 12$, 18, 24 and 30. We fixed $d_1/D = 0.663$ where the effect of the inner tubes is optimized for the confinement loss. We can see from Fig. 4(a) that increasing n_2 generally weakens the bend-induced loss for a given d_2/D. However, having more tubes in the outer ring limits the maximum achievable d_2/D, which restricts the overall reduction in the bend-induced loss. For $n_2 = 12$, local loss peaks are present at large d_2/D values. Here, the bending causes a coupling between the fundamental mode and one of the modes in the outer ring tubes, leading to light leakage from the core. This is evident from the 3-dB contour plot of the intensity profile at $d_2/D = 0.667$ presented in the inset in Fig. 4(a). The minimum bend-induced loss is realized when $n_2 = 12$ and $d_2/D = 0.5$. We recall from our earlier study in Fig. 2(b) that the optimum d_2/D for the straight fiber is 0.667. However, as shown in Fig. 4(a), this value is unsuitable for suppressing the bend-induced loss. To minimize the loss in a 7-cm bending, d_2/D of 0.5 should be used.

Let us now fix d_2/D at its optimum value of 0.5 in DR-NCF, and examine the bending loss performance for a varying d_1/D, as plotted in Fig. 4(b). Notice that the loss increases substantially at around $d_1/D = 0.773$. Here, the bending causes the fundamental mode to phase match with
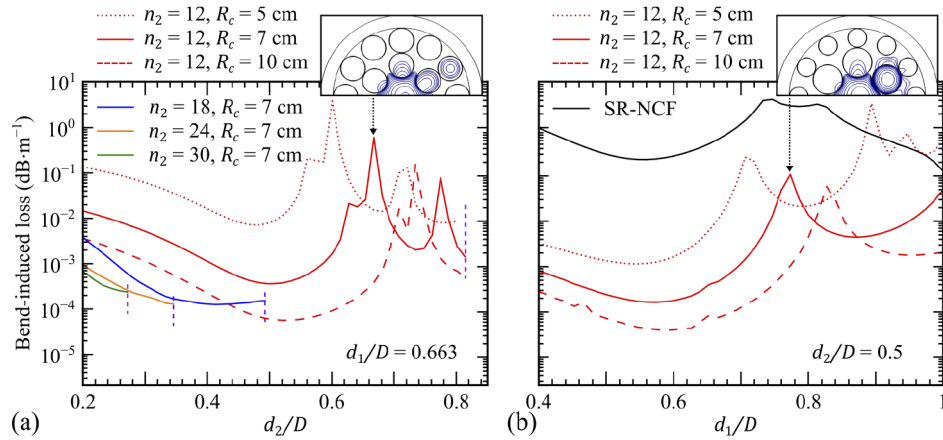
Fig. 4. (a) Bend-induced loss in the fundamental mode as a function of d_2/D for DR-NCF with $n_2 = 12$, 18, 24 and 30. The optimum $d_1/D = 0.663$ obtained from Fig. 2(a) is used. The inset is the 3-dB contour plot of the intensity profile showing the light leakage from the core into one of the outer antiresonant tubes when $d_2/D = 0.667$. The best bending performance at $R_c = 7$ cm is observed when $d_2/D = 0.5$. (b) Bend-induced loss as a function of d_1/D while n_2 and d_2/D are set at 12 and 0.5, respectively. The inset is the 3-dB contour plot of the intensity profile showing the light leakage from the core into one of the inner antiresonant tubes when $d_1/D = 0.773$. The bending performance of a six-tube SR-NCF as a function of d_1/D is presented as a reference. The bend-induced loss plotted for $R_c = 5$ cm and 10 cm when $n_2 = 12$ clearly demonstrate the effect of changing bending radius.

one of the modes in the inner ring tubes, resulting in a strong mode coupling between them. This leads to a large light leakage from the fundamental mode to the cladding mode as illustrated with a 3-dB contour plot of the intensity profile in the inset in Fig. 4(b). On the contrary, the fiber becomes much less sensitive to the bending in the range $0.5 < d_1/D < 0.7$. We note that there is a significant overlap between this and the range of d_1/D for achieving low-loss in the straight fiber as observed in Fig. 2(a). This means that we have a relatively large range for the choice of d_1/D that exhibit low loss, and at the same time, not too prone to bending. The bend-induced loss for a six-tube SR-NCF is presented in Fig. 4(b) as a reference. More than two orders of magnitude reduction in the bend-induced loss is achievable simply by introducing the second ring of antiresonant tubes.

At different bending radii, we observed shift of the entire curves in Fig. 4—to the left for a smaller bending radius, and vice versa. For example, as shown in Fig. 4(a), for $n_2 = 12$ and $d_1/D = 0.663$, the bend-induced loss minimum shifts to 0.48 and 0.513 for 5-cm and 10-cm bending radii, respectively.

5. Single-modedness

The presence of an additional ring of antiresonant tubes offers an extra set of parameters for controlling the single-modedness in the negative-curvature fiber. Figure 5(a) shows d_2/D dependence of the higher-order mode extinction ratio (HOMER) for $n_2 = 12$, 18, 24 and 30, while d_1/D is set at 0.663. HOMER is defined as the ratio between the lowest loss in the higher-order modes and loss in the fundamental mode. It is a measure of the light leakage in the higher-order modes with respect to that of the fundamental mode. In general, HOMER should be greater than 10 for a hollow-core fiber to remain effectively single mode.

As a reference, HOMER for a six-tube SR-NCF with $d_1/D = 0.663$ is marked with a horizontal-dashed line in Fig. 5(a). Within the range of n_2 and d_2/D that we studied, HOMER for DR-NCF
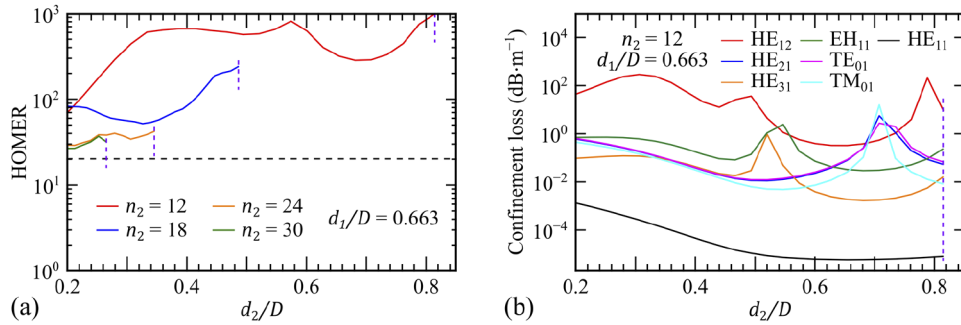
Fig. 5. (a) Higher-order mode extinction ratio (HOMER) for DR-NCF as a function of d_2/D for $n_2 = 12$, 18, 24 and 30, while d_1/D is set at 0.663. (b) The confinement loss of several higher-order modes as a function of d_2/D for DR-NCF with $n_2 = 12$ and $d_1/D = 0.663$.

is always greater than that of SR-NCF, suggesting that adding the second ring of antiresonant tubes enhances the single-modedness of the fiber. In particular, when $n_2 = 12$, the fiber exhibits excellent single-modedness (HOMER > 100) over a wide range of d_2/D, i.e. from 0.3 all the way up to where the outer tubes are in contact with each other.

Let us look at the modal property for the case when $d_1/D = 0.663$ and $n_2 = 12$ in more detail. Figure 5(b) shows the confinement loss of several higher-order modes (HE_{12}, HE_{21}, HE_{31}, EH_{11}, TE_{01}, TM_{01}) and the fundamental mode (HE_{11}). In the entire range of d_2/D studied, either HE_{31} or TM_{01} is the higher-order mode with the lowest loss. Beyond $d_2/D = 0.573$, HE_{31} is the least leaky higher-order mode, which is responsible for the decreasing HOMER up to $d_2/D = 0.787$ observed in Fig. 5(a). In this regard, we point out an earlier study, which revealed that a seven-tube arrangement efficiently suppresses the higher-order modes in SR-NCF [4]. We expect that the single-modedness can be further improved when seven inner antiresonant tubes are used instead of six in DR-NCF.

6. Fabrication tolerance

From the practical point of view, it is important to assess the susceptibility of the fiber performance to unintentional deviations in its final geometry that may develop in the fabrication process. For DR-NCFs, the most likely source of the flaw is at the contact points between the adjacent tubes in the inner and outer rings marked with red crosses in Fig. 1(a). Namely, the two circular antiresonant tubes will not be able to retain the ideal single contact point, but create an edge with a finite length as illustrated in Fig. 6(a). The thickness of the edge will be $2t$ due to the mass preservation. Similar edges can also be observed in negative-curvature fibers whose cladding elements are in contact with the neighboring ones, e.g. ice-cream-cone-cladding fiber [14]. Here, we quantify the percentage fabrication error by taking the length of the edge as a fraction of the circumference of the inner tube.

Figure 6(b) presents the comparison of the confinement loss over 0.9–1.6-µm bandwidth between the ideal DR-NCF with $n_2 = 12$, $d_1/D = 0.663$ and $d_2/D = 0.667$ and those with 5%, 7% and 10% fabrication-induced errors. Since $D = 30$ µm in our example, 5% error translates to the edge length of 3.12 µm. In practice, the fabrication error can be minimized by adequately placing support tubes in the gaps between the antiresonant tubes, as well as optimizing the drawing parameters, such as the drawing temperature, cladding tube pressure, feed and pull speeds. Our calculations show that the edges have a negative impact on the confinement loss, particularly towards the short-wavelength edge of the transmission window. At 1.06-µm wavelength, the confinement loss increases by about an order of magnitude for 5% fabrication error when
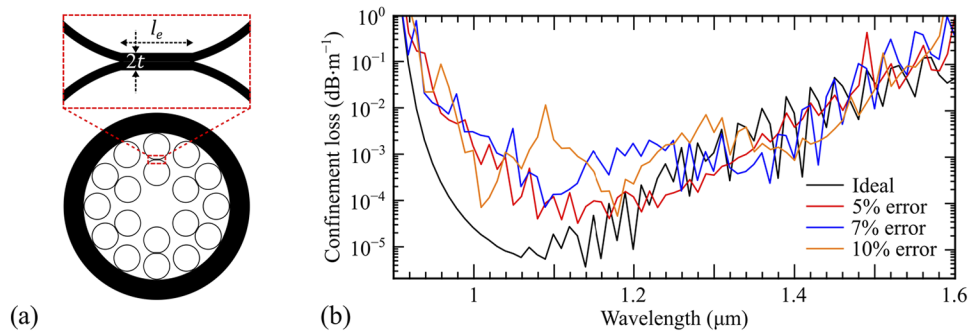
Fig. 6. (a) Illustration of the edge formation between the adjacent antiresonant tubes in the inner and outer rings caused by the fabrication imperfection. (b) Comparison of the confinement loss between the ideal DR-NCF (black, $n_2 = 12$, $d_1/D = 0.663$ and $d_2/D = 0.667$) and those with the fabrication-induced deformations (blue, green and red, 5%, 7% and 10% errors, respectively). We define the percentage fabrication error as the length of the edge as a fraction of the circumference of the inner tube, i.e. $l_e/\pi d_1 \times 100\%$

compared with the ideal structure. Nevertheless, this is still significantly lower than that of the ideal SR-NCF, CTF and NANF shown in Fig. 3.

7. Conclusions

We studied numerically the effect of introducing the second ring of antiresonant tubes in the negative-curvature fiber. Within the double-ring design framework studied here, we can conclude that $n_2 = 12$ and $d_2/D = 0.5$ or $n_2 = 18$ and $d_2/D = 0.44$ are the best choice for the second ring structural parameters, considering the confinement loss, bend-induced loss and single-modedness. Up to four orders of magnitude improvement in the confinement loss can be obtained by simply adding another layer of antiresonant tubes. Our calculations show that DR-NCF can outperform NANF and CTF that recently achieved record-low loss values, however, at an expense of reduced transmission bandwidth. Furthermore, DR-NCF exhibits much better bending loss and single-modedness compared to its single-ring counterpart. At 5% fabrication-induced error, the confinement loss in DR-NCF increases by approximately an order of magnitude. However, it still exhibits excellent guidance relative to the other single-cladding layer designs. We believe these findings will stimulate, and serve as an excellent guideline for, its experimental realization.

Funding

Disclosures

The authors declare no conflicts of interest.

References

1. R. F. Cregan, B. J. Mangan, J. C. Knight, T. A. Birks, P. S. J. Russell, P. J. Roberts, and D. C. Allan, "Single-mode photonic band gap guidance of light in air," Science **285**(5433), 1537–1539 (1999).
2. F. Couny, F. Benabid, and P. S. Light, "Large pitch kagomé-structured hollow-core photonic crystal fiber," Opt. Lett. **31**(24), 3574–3576 (2006).
3. F. Poletti, N. V. Wheeler, M. N. Petrovich, N. Baddela, E. Numkam Fokoua, J. R. Hayes, D. R. Gray, Z. Li, R. Slavík, and D. J. Richardson, "Towards high-capacity fibre-optic communications at the speed of light in vacuum," Nat. Photonics **7**(4), 279–284 (2013).

4. M. Michieletto, J. K. Lyngsø, C. Jakobsen, J. Lægsgaard, O. Bang, and T. T. Alkeskjold, "Hollow-core fibers for high power pulse delivery," Opt. Express **24**(7), 7103–7119 (2016).
5. P. S. J. Russell, P. Hölzer, W. Chang, A. Abdolvand, and J. C. Travers, "Hollow-core photonic crystal fibres for gas-based nonlinear optics," Nat. Photonics **8**(4), 278–286 (2014).
6. M. R. A. Hassan, F. Yu, W. J. Wadsworth, and J. C. Knight, "Cavity-based mid-IR fiber gas laser pumped by a diode laser," Optica **3**(3), 218–221 (2016).
7. M. I. Hasan, N. Akhmediev, A. Mussot, and W. Chang, "Midinfrared pulse generation by pumping in the normal-dispersion regime of a gas-filled hollow-core fiber," Phys. Rev. Appl. **12**(1), 014050 (2019).
8. L. Vincentti and V. Setti, "Waveguiding mechanism in tube lattice fibers," Opt. Express **18**(22), 23133–23146 (2010).
9. Y. Y. Wang, N. V. Sheeler, F. Couny, P. J. Roberts, and F. Benabid, "Low loss broadband transmission in hypocycloid-core Kagome hollow-core photonic crystal fiber," Opt. Lett. **36**(5), 669–671 (2011).
10. F. Poletti, "Nested antiresonant nodeless hollow core fiber," Opt. Express **22**(20), 23807–23828 (2014).
11. M. I. Hasan, N. Akhmediev, and W. Chang, "Positive and negative curvatures nested in an antiresonant hollow-core fiber," Opt. Lett. **42**(4), 703–706 (2017).
12. C. Wei, J. Weiblen, C. R. Menyuk, and J. Hu, "Negative curvature fibers," Adv. Opt. Photonics **9**(3), 504–561 (2017).
13. A. D. Pryamikov, A. S. Biriukov, A. F. Kosolapov, V. G. Plotnichenko, S. L. Semjonov, and E. M. Dianov, "Demonstration of a waveguide regime for a silica hollow - core microstructured optical fiber with a negative curvature of the core boundary in the spectral region > 3.5 μm," Opt. Express **19**(2), 1441–1448 (2011).
14. F. Yu, W. J. Wadsworth, and J. C. Knight, "Low loss silica hollow core fibers for 3–4 μm spectral region," Opt. Express **20**(10), 11153–11158 (2012).
15. A. N. Kolyadin, A. F. Kosolapov, A. D. Pryamikov, A. S. Biriukov, V. G. Plotnichenko, and E. M. Dianov, "Light transmission in negative curvature hollow core fiber in extremely high material loss region," Opt. Express **21**(8), 9514–9519 (2013).
16. L. Vincetti and V. Setti, "Extra loss due to Fano resonances in inhibited coupling fibers based on a lattice of tubes," Opt. Express **20**(13), 14350–14361 (2012).
17. W. Belardi and J. C. Knight, "Hollow antiresonant fibers with reduced attenuation," Opt. Lett. **39**(7), 1853–1856 (2014).
18. B. Debord, A. Amsanpally, M. Chafer, A. Bas, M. Maurel, J. M. Blondy, E. Hugonnot, F. Scol, L. Vincetti, F. Gérome, and F. Benabid, "Ultralow transmission loss in inhibited-coupling guiding hollow fibers," Optica **4**(2), 209–217 (2017).
19. S. F. Gao, Y. Y. Wang, W. Ding, D. L. Jiang, S. Gu, X. Zhang, and P. Wang, "Hollow-core conjoined-tube negative-curvature fibre with ultralow loss," Nat. Commun. **9**(1), 2828 (2018).
20. T. D. Bradley, J. R. Hayes, Y. Chen, G. T. Jasion, S. R. Sandoghchi, R. Slavík, E. Numkam Fokoua, S. Bawn, H. Sakr, I. A. Davidson, A. Taranta, J. P. Thomas, M. N. Petrovich, D. J. Richardson, and F. Poletti, "Record low-loss 1.3 dB/km data transmitting antiresonant hollow core fibre," *2018 European Conference on Optical Communication (ECOC)*, Rome, 2018, pp. 1–3.
21. X. Huang, S. Yoo, and K. T. Yong, "Function of second cladding layer in hollow-core tube lattice fibers," Sci. Rep. **7**(1), 1618 (2017).
22. S. Yan, S. Lou, W. Zhang, and Z. Lian, "Single-polarization single-mode double-ring hollow-core anti-resonant fiber," Opt. Express **26**(24), 31160–31171 (2018).
23. X. Chen, X. Hu, L. Yang, J. Peng, H. Li, N. Dai, and J. Li, "Double negative curvature anti-resonance hollow core fiber," Opt. Express **27**(14), 19548–19554 (2019).
24. G. J. Pearce, G. S. Wiederhecker, C. G. Poulton, S. Burger, and P. S. J. Russell, "Models for guidance in kagome-structured hollow-core photonic crystal fibres," Opt. Express **15**(20), 12680–12685 (2007).
25. M. Alharbi, T. Bradely, B. Debord, C. Fourcade-Dutin, D. Ghosh, L. Vincetti, F. Gérôme, and F. Benabid, "Hypocycloid-shaped hollow-core photonic crystal fiber Part II: Cladding effect on confinement and bend loss," Opt. Express **21**(23), 28609–28616 (2013).
26. X. Huang, W. Qi, D. Ho, K. T. Yong, F. Luan, and S. Yoo, "Hollow core anti-resonant fiber with split cladding," Opt. Express **24**(7), 7670–7678 (2016).
27. S. Yan, S. Lou, X. Wang, W. Zhang, and T. Zhao, "Single-mode large-mode-area double-ring hollow-core anti-resonant fiber for high power delivery in mid-infrared region," Opt. Fiber Technol. **46**, 118–124 (2018).
28. R. T. Schermer and J. H. Cole, "Improved bend loss formula verified for optical fiber by simulation and experiment," IEEE J. Quantum Electron. **43**(10), 899–909 (2007).